Article

Current Biology

Valence and State-Dependent Population Coding in Dopaminergic Neurons in the Fly Mushroom Body

Highlights

- Custom 3D image registration method to analyze neuronal population imaging data
- Fly dopamine neuron population encodes innate valence of odors or tastes
- DAN compartment activity is modulated by different physiological states
- DAN compartment activity correlates with movement conveying behavioral state

Authors

K.P. Siju, Vilim Štih, Sophie Aimon, Julijana Gjorgjieva, Ruben Portugues, Ilona C. Grunwald Kadow

Correspondence

ilona.grunwald@tum.de

In Brief

Dopamine has been studied extensively in its role as a reward signal during learning across animal species. Taking advantage of the confined anatomy of DANs innervating the mushroom body (MB) of the fly, Siju et al. show that DAN populations encode innate odor and taste valence, movement, and physiological state in a MB-compartment-specific manner.

Siju et al., 2020, Current Biology *30*, 2104–2115
June 8, 2020
https://doi.org/10.1016/j.cub.2020.04.037

CellPress

CellPress
OPEN ACCESS

Current Biology

Article

Valence and State-Dependent Population Coding in Dopaminergic Neurons in the Fly Mushroom Body

K.P. Siju,[1] Vilim Štih,[2] Sophie Aimon,[1] Julijana Gjorgjieva,[1,3] Ruben Portugues,[2,4,5] and Ilona C. Grunwald Kadow[1,6,7,*]
[1]TUM School of Life Sciences, Technical University of Munich, 85354 Freising, Germany
[2]Sensorimotor Control Group, Max Planck Institute of Neurobiology, 82152 Martinsried, Germany
[3]Computation in Neural Circuits Group, Max Planck Institute for Brain Research, 60438 Frankfurt am Main, Germany
[4]Institute of Neuroscience, Technical University of Munich, 80802 Munich, Germany
[5]Munich Cluster for Systems Neurology (SyNergy), 80802 Munich, Germany
[6]ZIEL–Institute of Food and Health, Technical University of Munich, 85354 Freising, Germany
[7]Lead Contact
*Correspondence: ilona.grunwald@tum.de
https://doi.org/10.1016/j.cub.2020.04.037

SUMMARY

Neuromodulation permits flexibility of synapses, neural circuits, and ultimately behavior. One neuromodulator, dopamine, has been studied extensively in its role as a reward signal during learning and memory across animal species. Newer evidence suggests that dopaminergic neurons (DANs) can modulate sensory perception acutely, thereby allowing an animal to adapt its behavior and decision making to its internal and behavioral state. In addition, some data indicate that DANs are not homogeneous but rather convey different types of information as a heterogeneous population. We have investigated DAN population activity and how it could encode relevant information about sensory stimuli and state by taking advantage of the confined anatomy of DANs innervating the mushroom body (MB) of the fly *Drosophila melanogaster*. Using *in vivo* calcium imaging and a custom 3D image registration method, we found that the activity of the population of MB DANs encodes innate valence information of an odor or taste as well as the physiological state of the animal. Furthermore, DAN population activity is strongly correlated with movement, consistent with a role of dopamine in conveying behavioral state to the MB. Altogether, our data and analysis suggest that DAN population activities encode innate odor and taste valence, movement, and physiological state in a MB-compartment-specific manner. We propose that dopamine shapes innate perception through combinatorial population coding of sensory valence, physiological, and behavioral context.

INTRODUCTION

Behavioral and internal states and past and current experience shape animal perception and behavior. Neuromodulators convey these states and contexts across brain regions and between body and brain [1–3]. Dopamine is among the most intensely studied signals that modulate neural processing and govern plasticity of synaptic connections [4–6]. In the mammalian brain, dopaminergic neurons (DANs) are located in clusters in several brain regions, including the mesencephalon, diencephalon, and olfactory bulb [7]. The most important sources of dopamine are arguably the *substantia nigra* and the ventral tegmental area (VTA), which send projections to the dorsal and ventral striatum, respectively. Brain dopamine has been implicated in cognitive (e.g., motivation, reinforcement, goal-directed behavior, motor control and movement, decision making, and learning) as well as more basic functions (e.g., reproduction and nausea) [4, 7]. How dopamine contributes to these different aspects of neural circuit function and behavior is an open question. A potential answer could lie in the highly localized and region-specific release of dopamine, depending on context and task the animal faces [8].

Invertebrates, including the fly *Drosophila melanogaster*, use dopamine in highly analogous processes [1, 6, 9]. The exquisite tools of fly genetics have provided important insights into the role and molecular and circuit mechanisms of dopamine in associative learning and memory as well as state-dependent behavior (e.g., [10–15]). A focus of many studies has been a dense network of ~200 dopaminergic cells innervating the mushroom body (MB) (Figure 1A), a brain structure organized in 15 interconnected neuronal compartments (i.e., α1–3, α'1–3, β1, β2, β'1, β'2, and γ1–5) (Figure 1B) [11, 16]. MB DANs, through unknown mechanisms, respond to stimuli of innate value, such as sweetness, heat, and electric shock, consistent with a model where they convey the "unconditioned stimulus" (US) during learning to MB intrinsic Kenyon cells (KCs) and their corresponding MB output neurons (MBONs) [17]. By taking advantage of highly specific transgenic techniques, recent studies have dissected the function of small subsets or even of single DANs in behavior (e.g., [18–27]). For example, the PPL1 subgroup of DANs, which innervate the α and α' lobes as well as γ1, γ2, and a region referred to as the peduncle, have been implicated in signaling negative US, such as punishment. In contrast, PAM DANs projecting to the β, β', and γ (i.e., γ4 and γ5) compartments appear

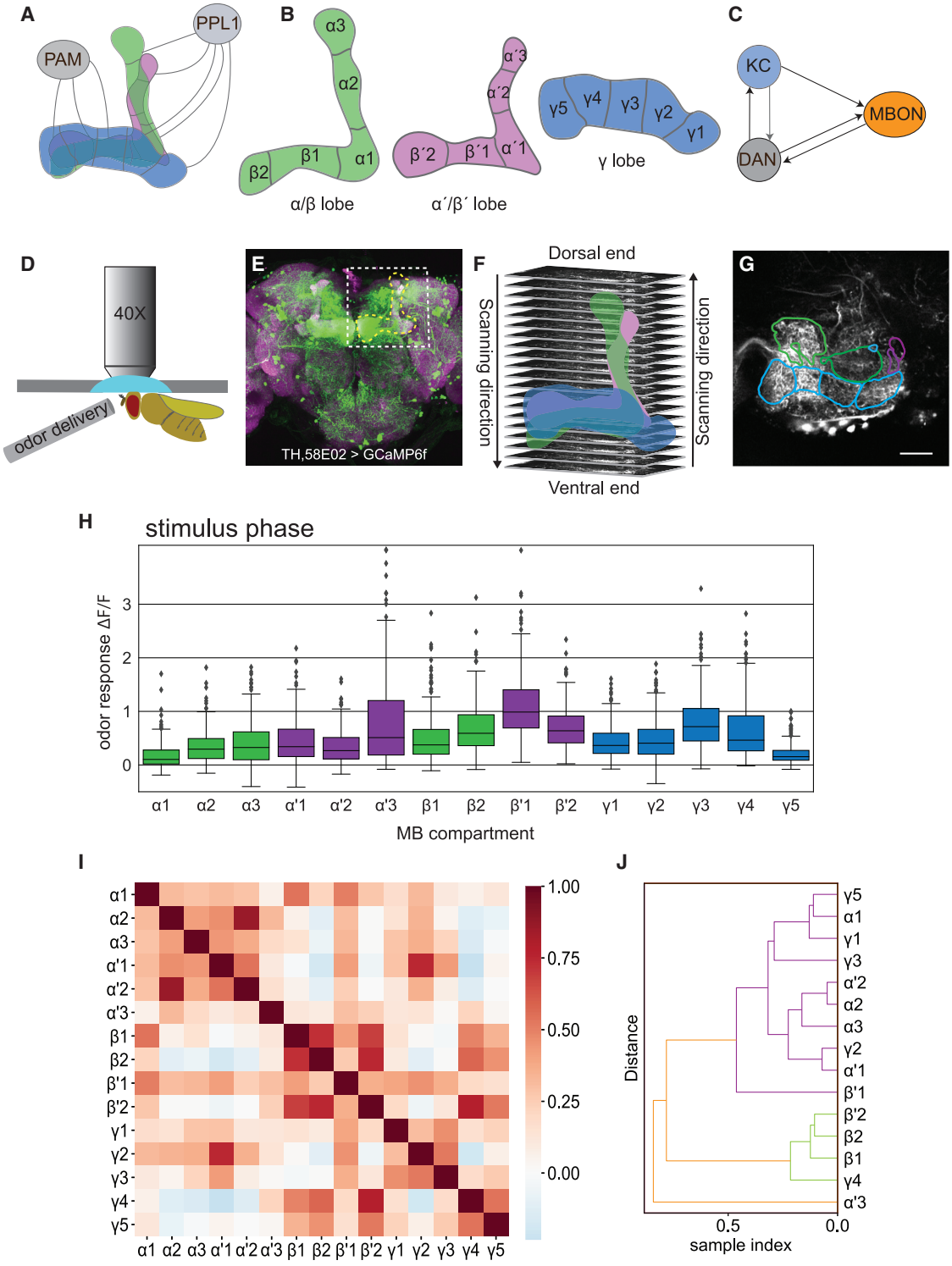

Figure 1. *In Vivo* Two-Photon Population Imaging of Mushroom Body Dopaminergic Neurons

(A) Scheme showing the mushroom body and innervating two clusters of dopaminergic neurons (PAM and PPL1).

(B) Schematics of the mushroom body lobes with 15 DAN compartments.

(C) Minimal circuit motif of the mushroom body depicting recurrent connections between dopaminergic cells (DANs), Kenyon cells (KCs), and mushroom body output neurons (MBONs).

(D) A schematic depicting the *in vivo* fly preparation for imaging at the two-photon microscope.

(legend continued on next page)

to provide a rewarding signal to KCs and MBONs during associative learning [10, 11] (Figure 1A).

As yet, less is known about the role of the different DAN types and their respective MB compartments during state-dependent (e.g., physiological states and movement) and innate sensory perception and behavior. Moreover, given that DANs are part of a highly interconnected recurrent network, we lack knowledge regarding their population activity and dynamics as compared to the numerous studies recording the isolated activity of individual DAN types. A notable exception, a study by Cohn et al., provided compelling evidence that relative activities of these neurons matter to US perception and behavior of the fly by analyzing simultaneous calcium signals of all neurons in a DAN subpopulation (~40 DANs) innervating the γ-lobe of the MB [28]. This study suggested that subtypes of DANs of different γ-compartments were highly coordinated or anti-correlated in a behavioral state- and context-dependent manner.

Interestingly, DANs respond to sensory stimuli, including odors and temperature changes, and contribute to sensory valence decisions in naive animals [18, 25, 28–32]. Consistently, electron microscopic connectomics data from fly larvae and adults suggest that DANs, especially their axon terminals, receive odor information by KCs as part of a recurrent circuit [33–35] (Figure 1C). Moreover, MBONs provide input to several DANs [34, 36, 37]. It is also conceivable that olfactory pathways from the lateral horn convey odor information to DANs innervating the MB [38]. These findings motivate the question of how populations of DANs contribute to sensory perception and valence decisions and how they convey state-dependent information. We have begun to address this complex question by recording primarily odor responses across all DANs innervating the fly's MB. In particular, we analyzed population-wide contributions of DANs to innate valence perception and state changes.

RESULTS

To this end, we setup an *in vivo* preparation to image calcium fluctuations in all DANs innervating the MB by using two-photon microscopy (*TH-Gal4,58E02-Gal4;UAS-GCaMP6f*) (Figures 1D and 1E). We recorded from a 210 × 210 pixels area with a resolution of 1 × 1 × 2 μm/pixel covering the entire MB structure in one hemisphere of the brain and stimulated every animal with two different odorants (e.g., odor 1 from dorsal to ventral and odor 2 from ventral to dorsal) (Figure 1F). To minimize bias or experimental artifacts, we varied odors as well as scanning direction. To average responses of DAN populations over many individual experiments and animals, we developed a method that allowed us to segment fluorescence changes into each of the 15-MB compartments and to align different brains in 3D (Figures 1C–1G and S7; see STAR Methods). In essence, we used the recently published 3D mask as a landmark for all MB compartments [11] to semi-automatically assign fluorescent changes in DAN axons of individual animals (Figures 1F and 1G). Importantly, this method enabled us to analyze the responses of the entire 3D volume and not only of a manually defined 2D region of interest for a given compartment. Recording from all DANs at sufficient spatial resolution required imaging the brain over multiple sections with repeated odor presentations of the same odor (see STAR Methods). With these caveats in mind, for this present study, we decided to focus on spatially distinct rather than temporally dynamic signals of MB DANs.

Using this setup, we imaged DAN responses in a total of 201 adult female flies for two out of 12 odorants (i.e., vinegar [Figure S1A], yeast, citronella, peppermint, 3-octanol, ethanol, 4-methylcyclohexanol, geosmin, isoamyl acetate, 1-hexanol, 2-heptanone, and 11-cis-vaccenyl acetate [cVA]) (Figure S1B). To allow for potential comparison, we chose an overlapping odor set to the one used by Hige et al. [39], who analyzed responses of individual MBONs in naive animals. Moreover, we recorded from flies of four different internal states, starved (24 and 48 h starved), fed, virgin, or mated, to assess the impact of hunger or mating state on DANs.

Combining all experiments from all flies and all odor stimuli and states, we first sought to determine how much of the observed variance in the recorded GCaMP fluorescence signal resulted from biological (e.g., odor stimulus, metabolic state, and MB compartment) as opposed to procedural factors (e.g., imaging direction, order or position of odor stimulus, etc.) (Table 1). Using an ANOVA model combining the different factors and their specific compartment effects, we determined that known procedural factors only accounted for a small part of the data variance. In essence, stimulus order (e.g., whether the odor was the first, second, etc. in a series presented to the animal), scanning direction (i.e., dorsal to ventral versus ventral to dorsal), and hence number of previously received olfactory stimuli had a significant effect and together explained up to 1% of the variance in the calcium signals (Table 1; Figure S1G). This could be indicative of some, albeit mild, adaptation due to repeated odor delivery. The highest contribution (~34%) to the observed variance came, importantly, from known biological factors (Table 1). Specifically, differences between the individual MB compartments as well as their response to a specific odorant explained over 30% of the observed variance in the data (Figure 1H; Table 1). Furthermore, we analyzed odor-stimulation-independent amplitude changes during the pre-stimulus phase (Figures S1C–S1F). Interestingly, the MB compartments with highest average deviations from zero in the pre-stimulus phase (i.e., α3 and α'1) were not the same compartments that showed the highest variance in their odor responses (i.e., α'3, β'1, and γ4). This implies that these variabilities are a biological feature of the respective

(E) A confocal projection image showing the expression pattern of TH,58E02 > GCaMP6f. GCaMP6f expression was visualized by anti-GFP (green) and neuropil by anti-discs large (magenta) immunostaining. Dotted yellow line indicates the mushroom body lobes and dotted white square the region imaged.
(F) Image showing the imaging planes and scanning directions from dorsal to ventral end covering vertical and horizontal mushroom body lobes.
(G) An imaging plane showing the 3D masks of the mushroom body lobes used for compartment segmentation and fluorescence extraction. Scale bar, 10 μm.
(H) Mushroom body compartmentwise odor response. All experiments over all odors, states, etc. were pooled.
(I) Correlation matrix of DAN odor responses in different compartments.
(J) Hierarchical clustering dendrogram of different compartments and their odor responses. All odors and conditions were pooled.
Box plots represent the 25th and 75th percentile, with the whiskers at 1.5 of the interquartile range. See also Figures S1 and S7 and Table 1.

Table 1. ANOVA Table Showing the Variance Associated with Different Factors

	Sum of Squares	% of Variance Explained	PR(> F)
MB compartment	313[a]	22.7[a]	0[a]
Stimulus	35[a]	2.5[a]	1.3E−36[a]
Compartment: stimulus	117[a]	8.4[a]	3.0E−62[a]
Order presented	1.1	0.08	1.2E−02
Compartment: order_presented	1.5	0.1	8.6E−01
Imaging direction	3.4	0.2	8.3E−06
Compartment: imaging direction	7.1	0.5	1.4E−04
Starvation state	2.5	0.2	1.2E−04
Compartment: starvation state	6.4	0.5	6.4E−04
Residual	891	65	

R^2 = 0.36. See also Figure S7.
[a]Most significant factors.

compartments and not a technical artifact that should conceivably affect baselines and stimulus responses equally in all compartments or possibly only in the most dorsal ones (i.e., α3 and α'3) (Figures S1D and S1G).

Hence, by considering the known and intended conditions of the experiments (i.e., odor identity, metabolic state, compartment identity, imaging direction, and position in odor sequence), we were able to explain ~36% of the observed variance in our data (R^2 = 0.36) (Table 1). The highest contribution came from the differences in activity of different MB lobes, indicating that distinct MB compartments display characteristic calcium responses (Table 1).

As mentioned above, DANs form part of a network with other neurons types, such as MBONs, which also connect them back to other DANs [11, 34]. In addition, some DANs innervate multiple compartments [11], suggesting that the activity of some MB compartment should be correlated. To test this, we first generated an "anatomical connectome" as a correlation matrix, with the caveat that it likely does not contain all possible connections between neurons, to be compared with a "functional connectome." For the anatomical matrix, which was based on that of Aso et al. [11], we assigned strong connectivity between compartments innervated by the same DAN and milder connectivity for compartments with DAN dendrite-dendrite colocalization, common inputs from KCs or KC axon-axon connections, and MBON feedback to DANs (see STAR Methods; Figures S1H and S1I). When comparing this correlation matrix to the correlation matrix obtained for correlated or anti-correlated activity between MB compartments (Figures 1I and 1J versus Figures S1H and S1I), we noticed some obvious similarities, indicating that some of the correlated activity can be explained by known anatomical connections (e.g., α'1 and γ2). Nevertheless, we noticed several highly correlated compartments that did not appear to share direct input (e.g., β1 and β'2), indicating the existence of additional connections or mechanisms coordinating the responses of these compartments, as indicated by recent higher resolution connectomics data (e.g., [34]).

We next asked whether and what type of information DAN responses contain about the odor stimulus and how it might be perceived by the animal. In order to visually compare responses to different odors, we plotted averaged odor responses over all animals that received a given stimulus in a 2D heatmap (Figures 2A and S2). Considering these average response heatmaps, we wondered whether DANs could help to encode odor identity in their population activity (Figure 2B). As indicated in Table 1, stimulus identity induced compartment-specific responses and in total accounted for 10.9% of the observed variance. Of note, the specific effects of the stimulus on different compartments explained a larger proportion of the variance than just stimulus alone (Table 1) (8.4% versus 2.5%), suggesting that different compartments might respond differentially to different stimuli. Decoding odor identity from the recorded DAN population activity by using logistic regression (see STAR Methods) indeed performed at about three times higher accuracy than chance level (29% versus 8% chance level) (see confusion matrix in Figure S2B). Consistent with this, odor representation in linear discriminant analysis (LDA) space (see STAR Methods) was not homogeneous, and the distance between each odor cluster was higher than if odor had been randomly shuffled (1.6 versus 0.8 ± 0.06) (see, for example, Figures 2C and 2D). Although DANs are not very good encoders of odor identity in the fly brain, these results suggest that their responses might still convey some potentially useful information about the type of odor that the animal is smelling. This information could, for instance, be conveyed by KCs, which possess the complexity to encode odor specificity [40]. The biological meaning of this is currently unclear, but it is possible that modulation of MB function through DANs is influenced by the identity or type of odor the animal smells.

Humans frequently rate odors, including novel scents, as pleasant or unpleasant [41]. In flies, DANs have been implicated in regulating innate olfactory preference behavior (e.g., [13, 15, 18, 42]). We therefore next looked for an innate valence code for odors in this neuron population. To this end, we focused on the odors reported to possess an innate valence in behavioral assays for the animal: the food odors vinegar and yeast were categorized as positive and citronella, geosmin, and peppermint as negative [43–46]. Using the same ANOVA model as above for this dataset but analyzing stimulus valence instead of stimulus identity (Table S1), we found that valence accounted for 3.6% of the observed variance as compared with 8.5% for stimulus identity for this dataset. This difference of 4.9% is consistent with the interpretation that DANs, in addition to valence, hold some further information about the nature of an odor stimulus (e.g., odor type).

Regarding odor valence, by examining post hoc pairwise comparisons and regression coefficients for individual compartments, we noticed that DANs innervating the α3, α'1, and γ2 compartments responded stronger to aversive odors than they did to appetitive odors (Figure 3A). Conversely, β2, β'2, and γ4 showed higher DAN responses for odors of positive valence compared with the odor of negative valence (Figure 3A). This division coincides with the PAM and PPL1 MB innervation boundary and their reported responses to stimuli of opposite innate valences, such as sugar, bitter tastes (see below), or electric shock [20, 27, 29]. Interestingly, by using logistic regression on the DAN

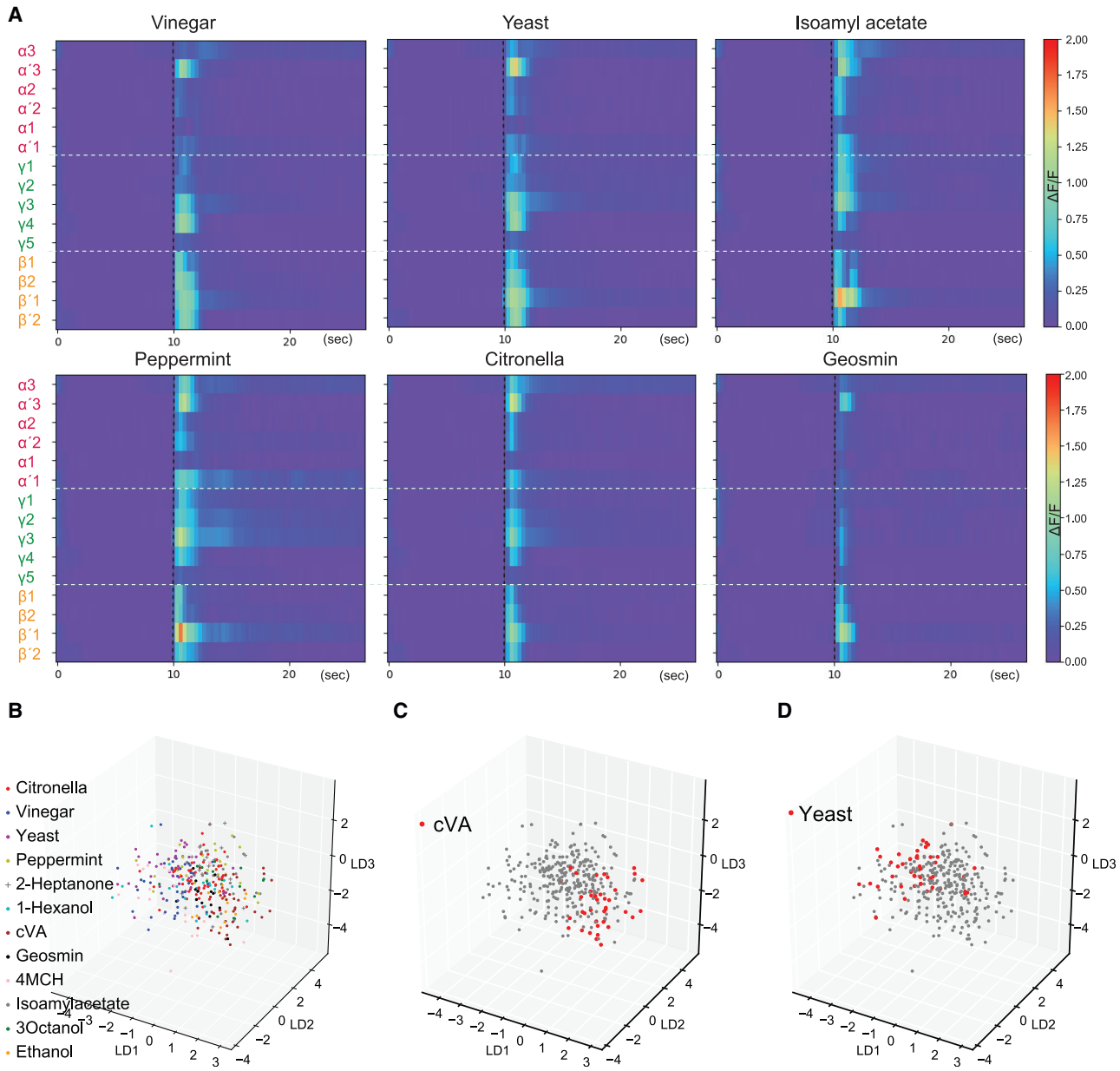

Figure 2. Dopamine Neuron Population Responses Contain Limited Information about Odor Identity

(A) Heatmaps showing averaged DAN responses to different odors in 15 mushroom body compartments (n = 369 experiments, 185 female flies). Vertical dashed black lines indicate stimulus delivery time. Horizontal dashed white lines separate the groups of lobes.

(B–D) State space after linear discriminant analysis dimensionality reduction. (B) presents all odors, and (C) and (D) highlight cVA and yeast.

See also Figure S2.

population activity data, the valence of an odor could indeed be decoded with significantly higher accuracy than chance level (70% versus 49%; $p = 0.0006$), suggesting that odor-evoked activity within the DAN network contributes to an animal's innate perception of odor valence (Figure 3B). Moreover, LDA loadings (the weights of the original data points in compartment space projected onto the LDA direction) were also segregated along opposite odor valences significantly more than LDA loadings obtained assigning valence randomly (Figures 3B and S3A) (d' = 1.29 compared with 0.60 ± 0.11 for random assignment; $p < 0.001$). LDA coefficients showed that DANs innervating different lobes contribute differentially to this segregation. The most significant contribution to odor valence classification was found for DANs projecting into the β'2 compartment (Figure 3C). To test the robustness of the valence signal within the DAN population, we ran the same analysis using the same 5 odors, but this time included also 3-octanol and 4-methylcyclohexanol, as these odors were reported to elicit innate aversion in some behavioral assays, which is, at least in part, dependent on specific MBONs [44, 47]. These odors are also frequently used to

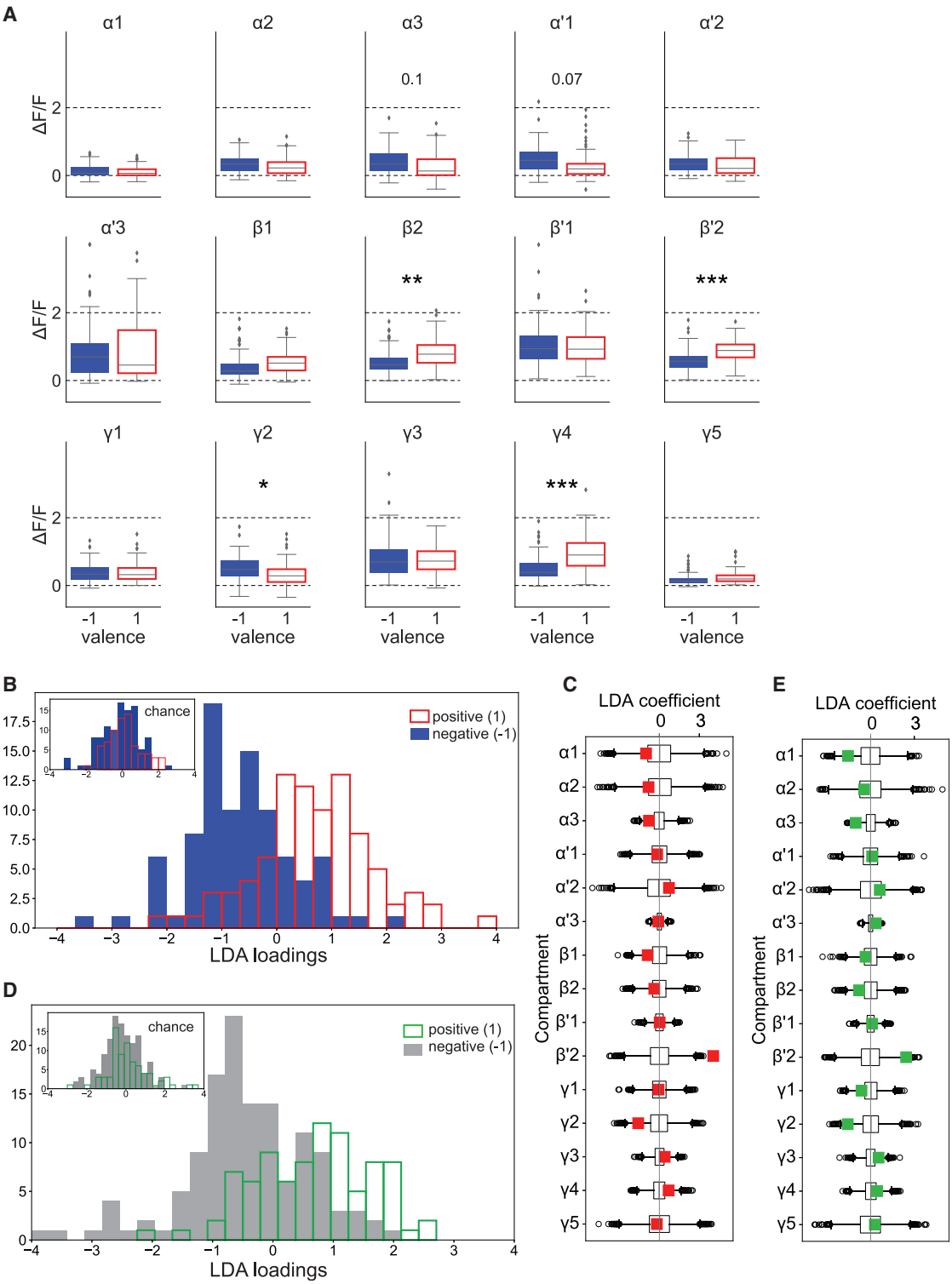

Figure 3. Dopamine Neuron Responses Reveal Innate Odor Valence

(A) Lobewise pairwise comparison of response to positive or negative valence odors. Stars represent t test multiple comparison corrected p values. *$p < 0.05$; **$p < 0.01$; ***$p < 0.001$.

(B) Histogram of loadings of projection on the valence-optimized LDA dimension for odors of high innate valence (vinegar, yeast, citronella, peppermint, and geosmin). The y axis represents counts per bin.

(C) Lobe coefficients for valence-optimized LDA in color for odors of high innate valence (vinegar, yeast, citronella, peppermint, and geosmin). Boxplots represent the distribution of coefficients obtained by chance.

(legend continued on next page)

study learning in flies. The results for the logistic regression of the DAN population data were very similar to the results without these two odors (69% classification accuracy versus 55% for chance; $p = 0.008$) (Figures 3D and S3B). LDA loadings were again segregated along opposite odor valences significantly more than LDA loadings obtained assigning valence randomly (Figure 3D) ($d' = 1.12$ compared with 0.55 ± 0.10 for random assignment; $p < 0.001$). Given earlier reports that odors (e.g., vinegar) can become less appetitive or even aversive to flies at high concentrations [46, 48], we next recorded DAN responses of flies to 32 ppm vinegar and compared them to the already recorded 4 ppm vinegar responses (Figure S3D). Although pairwise comparison of compartment-specific DAN responses revealed a significant difference in β'1 and γ1 (Figure S3D), we did not observe any significant changes in other compartments, such as β'2 or γ2, suggesting that high and low vinegar concentrations might not be perceived as different in valence at the level of DANs but possibly different in intensity. To comprehend these results better, we analyzed the preference behavior of flies of the same genotype as used from imaging to these two vinegar concentrations in a 4-quadrant olfactory arena [15, 18]. In our hands, and under the used conditions, when flies were given a direct choice between the high and the low vinegar concentration, flies displayed indifference (Figure S3E). Similarly, flies preferred not only 4 ppm vinegar over humidified air, they also favored 32 ppm vinegar odor over air. Thus, the DAN population response matched the animals' innate attraction to the odors.

Together, these data provide new insights into how the population of DANs could contribute to innate valence perception of odors, as previously observed in behavioral studies [13, 18].

As for odors, animals also have innate preferences for tastes, and previous work showed that certain DANs respond to sugar or bitter substances [27]. We next carried out DAN population imaging to analyze (1) which DANs respond to aversive versus attractive tastes and (2) to compare our odor valence data with another sensory stimulus. To avoid repeated stimulations with tastes, because they stick to the fly's legs and proboscis and are being ingested, we opted for another microscopy method, light-field microscopy (see STAR Methods and Figures S4A and S4B). Light-field imaging captures activity from the whole fly brain without the need for layered scanning [49] at a lower but still sufficient spatial resolution to capture the calcium dynamics in different DAN compartments (Figures S4A and S4B). Tethered flies expressing GCaMP6f in all DANs were alternatingly stimulated with the bitter taste quinine or sugar (Figure 4A). Remarkably, regression analysis revealed a highly similar distribution of coefficients as seen for odors of different innate valence (Figures 4B and S3A), suggesting that DANs encode valence of odors and taste in a very similar pattern. The clearest difference in representation of odor valence as compared to taste valence was seen in the γ-compartments, i.e., γ4 and γ5 (Figures 4B and S3A). Although γ4 was highly correlated with positive odor valence, γ5 displayed a high correlation for sugar (Figures 4B and S3A), consistent with previous reports [27, 28]. These data taken together, nevertheless, suggest that valence representation in the MB DAN population is mostly independent of the sensory modality. Furthermore, sugar is highly nutritive and the strong correlation in the γ5 compartment could, at least in part, represent the increased positive valence because of the calorie content of sugar and its long-lasting post-ingestion effects [50, 51].

Metabolic state is an important determinant in odor perception for many animals, including humans [52–54]. We thus compared DAN odor responses of fed with the responses of 24 and 48 h starved animals (Figure 5A). Metabolic state indeed contributed significantly, albeit less than stimulus valence, to the variance explained in the ANOVA analysis on the basis data from all test odors and all recorded animals (0.7%) (Table 1). Both post hoc pairwise comparisons and regression coefficients indicated that not all compartments contributed equally. We detected the most significant differences in responses in compartments α1, β1, β'2, and γ4 (Figures 5A and S5A). Previous studies that focused on individual DANs implicated some of these compartments in metabolic-state-dependent choice behavior (i.e., β'2) [13, 18, 55]. Our present results suggest that other compartments, such as β1, might also contribute in conveying feeding state to sensory processing. Importantly, decoding the responses of the entire DAN population allowed us to predict whether the fly was starved or fed with a 65% accuracy significantly higher than chance (65% versus 57%; $p = 0.04$). LDA projections as done above for odor valence segregated between starved and fed animals (Figure 5B) ($d' = 1.01$ compared with 0.49 ± 0.09 for random assignment). Interestingly, no single compartment stood out from chance levels in the LDA coefficients, suggesting that representation of metabolic state is distributed in the DAN population (Figure 5C). In addition, we detected a significant modulation of baseline activity (in the absence of an odor stimulus) by starvation in the γ4 compartment (Figures S5B and S5C). Of note, this modulation was not consistent between 24 and 48 h starved flies, and hence, its putative biological meaning remains unclear.

Altogether, the results suggest that feeding state modulates the response of DANs to odors, which in turn convey the animal's feeding state to different MB compartments.

One of the odors in our stimuli set was the sex pheromone cVA. Mating experience changes how males and females perceive their environments and members of their own species (e.g., [23, 56–58]). Thus, we compared cVA DAN responses in mated females with those of virgins. In particular, DANs projecting into compartments α3 and β'1 predicted mating state in a regression model (Figures S5E and S5F). By contrast, ANOVA showed that the pre-stimulus deviation from baseline was not significantly different in mated females as compared with virgins in the absence of an odor stimulus (Figure S5G). These results suggest that distributed activity in the DAN population shapes odor processing in the higher brain in a reproductive-state-dependent manner.

(D) Histogram of loadings of projection on the valence-optimized LDA dimension for odors vinegar, yeast, citronella, peppermint, geosmin, 3-octanol, and 4-methylcyclohexanol. The y axis represents counts per bin.

(E) Lobe coefficients for valence-optimized LDA in color for vinegar, yeast, citronella, peppermint, geosmin, 3-octanol, and 4-methylcyclohexanol. Boxplots represent the distribution of coefficients obtained by chance.

Box plots represent the 25th and 75th percentile, with the whiskers at 1.5 of the interquartile range. See also Figure S3 and Table S1.

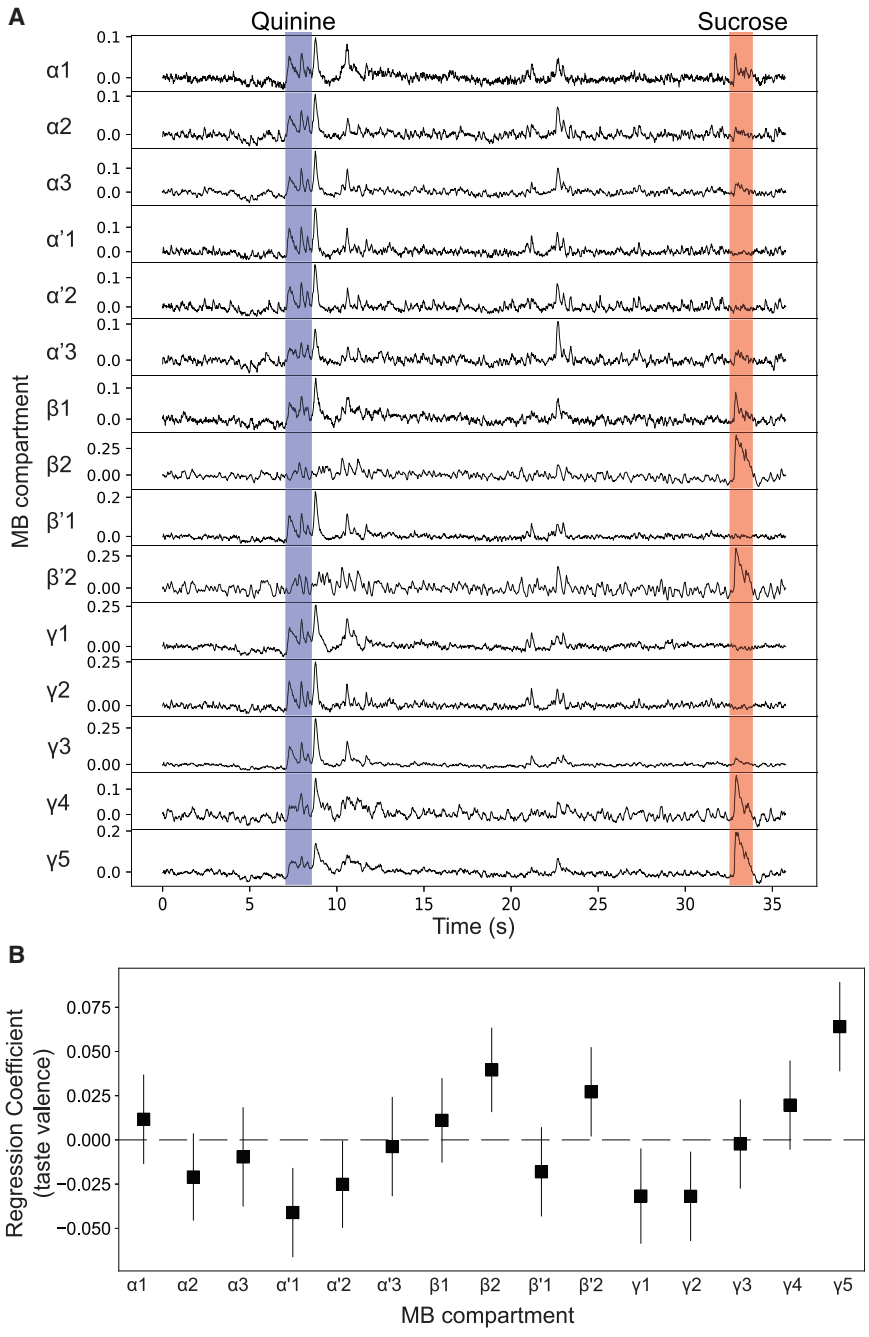

Figure 4. DANs Innervating Different MB Compartments Respond Differentially to Sweet and Bitter

(A) Sample traces of responses to quinine (bitter, blue) and sugar (red) taste collected with the light-field microscope. Shaded areas represent stimulus presentation. Note that the strong activity transient when quinine was removed is present in some datasets, but not all, and could be because of quinine wetting the legs.

(B) Regression coefficient for specific mushroom body compartments for tastes of innate valence (98% confidence interval).

See also Figure S4.

Given that some DAN responses were shown to be correlated with behavioral activity of the fly, independent of an external sensory stimulus, we wondered whether and where movement-related activity was encoded by the MB DAN population [28, 49, 59]. To test this, we analyzed another dataset of tethered flies walking on a ball but which were not stimulated with odor. These data were obtained by using light-field microscopy, allowing us to image calcium signals induced by walking at a very high temporal resolution across all compartments [49]. Walking was defined as movement on a ball, excluding behaviors such as grooming or proboscis extension. We then used regression of compartment fluorescence on these behavioral time series to obtain regression coefficients. We found that some MB compartments were strongly responsive to walking movement (Figures S6A–S6C). In particular, regression analysis indicated that calcium signals in compartments β1, β2, β'2, and γ3–5 correlated with walking (Figures S6B and S6C). The average regression coefficients for walking ranged from 0.01 to 0.07 (Figure S6C), which was similar (although possibly underestimated; see STAR Methods) to the coefficients observed for metabolic state (0–0.13) (Figure S5A), mating (0.01–0.38) (Figure S5F), and valence (−0.12–0.21) (Figure S3A). These data imply that movement is encoded by the MB DAN population and might affect an animal's sensory perception to, at least, a similar degree as other internal states. Whether and how walking speed, direction, intent, or even flying is represented in DANs will be an interesting question to be addressed in the future.

DISCUSSION

Altogether, we find that different DANs within the population of MB-innervating neurons respond differentially to different odors, tastes, and states and encode information regarding valence and physiological state in a compartment-specific manner (Figure 6). Different compartments show strongest responses during sensory stimulation, although others display highest baseline variability in the absence of stimuli (Figure 6). Furthermore, some compartments are clearly modulated while the animal is walking (Figure 6). Similarly, odor or taste valence is encoded more reliably by certain compartments than others when comparing DAN responses across the entire MB DAN population (Figure 6). And finally, metabolic and reproductive states modulate odor responses of the DAN population; DANs innervating some compartments again showed significantly higher effects

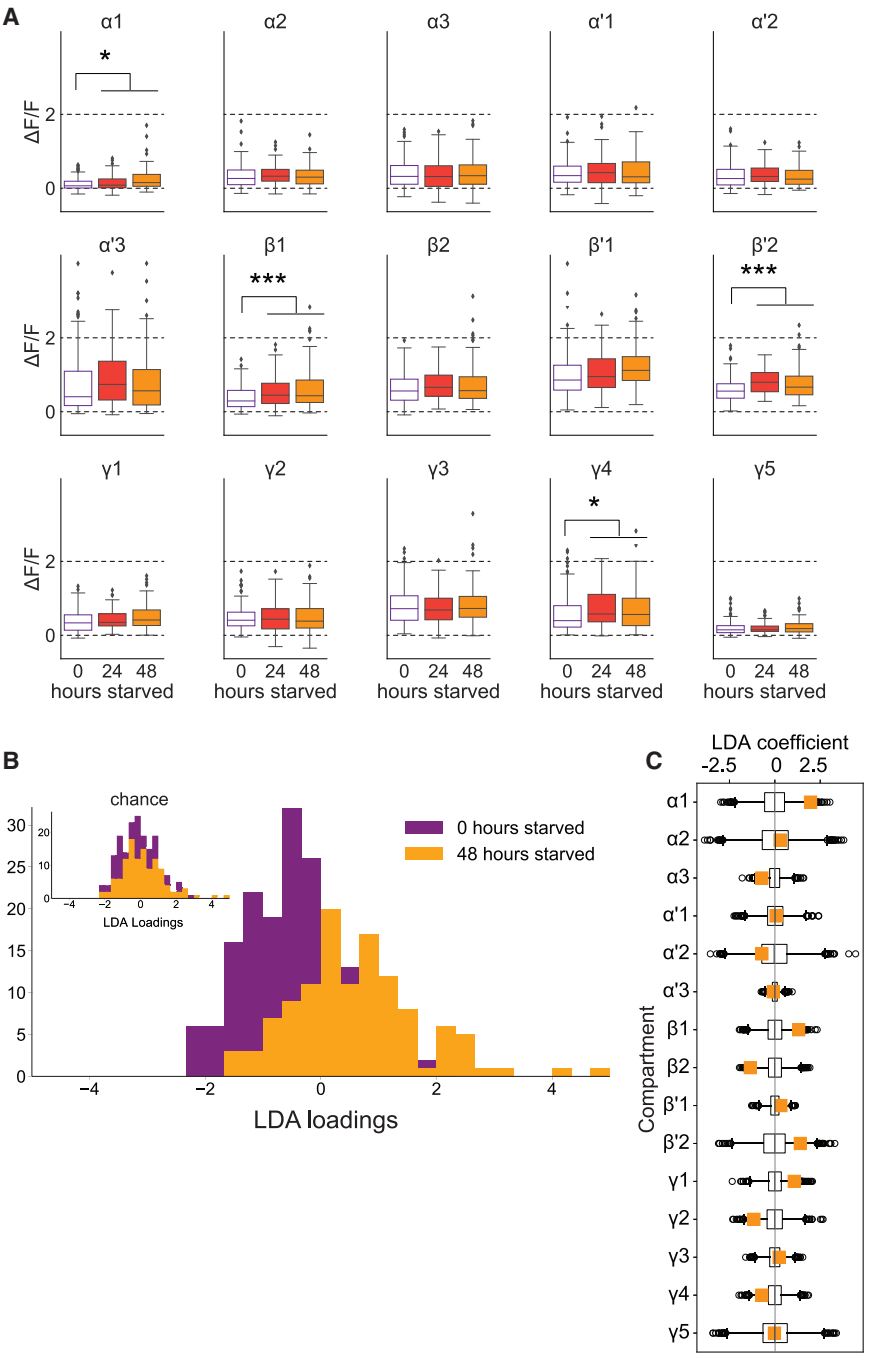

Figure 5. Metabolic State Affects Dopamine Neurons in Specific Mushroom Body Compartments

(A) Lobewise comparison of odor responses in different starvation states. Stars represent t test multiple comparison corrected p values. *$p < 0.05$; **$p < 0.01$; ***$p < 0.001$.

(B) Histogram of loadings of projection on the starvation-state-optimized LDA dimension. The y axis represents counts per bin.

(C) Lobe coefficients for metabolic-state-optimized LDA in color. Boxplots represent the distribution of coefficients obtained by chance.

Box plots represent the 25th and 75th percentile, with the whiskers at 1.5 of the interquartile range. See also Figure S5.

of modulation than others (Figure 6). On the basis of our analysis and modeling, we suggest that valence or the animal's state is encoded by a heterogeneous population of DANs, distributed and interconnected over multiple compartments, rather than by the activity of single neurons or single compartments.

A putative caveat in our data was the observed large variance that cannot be explained with known or controlled variables (Table 1). This variance, however, could be consistent with the finding that different individual flies respond differently to odors and state changes, resulting in the considerable variability typically observed in innate preference behavioral experiments. Of note, we saw similar variance in taste responses by using light-field imaging, indicating that the level of response variability is not merely due to technical factors. It is possible that individual experience shapes odor responses as suggested for variance observed in MBONs of different flies [39]. Alternatively, stochastic processes during development could lead to different wiring of neurons in individual flies [60], ultimately shaping how DANs respond to a given odor. Similarly, although the animals' legs were fully restrained in all imaging experiments (except for the taste and movement response analysis), small movements or the intent to move could conceivably influence DAN responses. Finally, we cannot exclude that differences in GCaMP expression and compartmental localization, as well as differences in fly preparation, contribute to the observed differences. We hope to answer how individuality shapes odor experience at the level of DANs in the future by combining higher throughput imaging methods with developmental genetics.

Importantly, in spite of putative individual differences, DANs as a population contain important information that could contribute markedly to the innate and state-dependent perception of odors and tastes, and possibly other sensory modalities, by gauging output pathways of the MB. More specifically, compartmentalized but population-wide DAN responses to odor or taste could bias MBON output by acutely modulating KC-MBON synapses. In this scenario, the odor information could be received from KC-DAN or MBON-DAN synapses directly but might also originate from the lateral horn (LH). In line with this idea, a valence bias has also

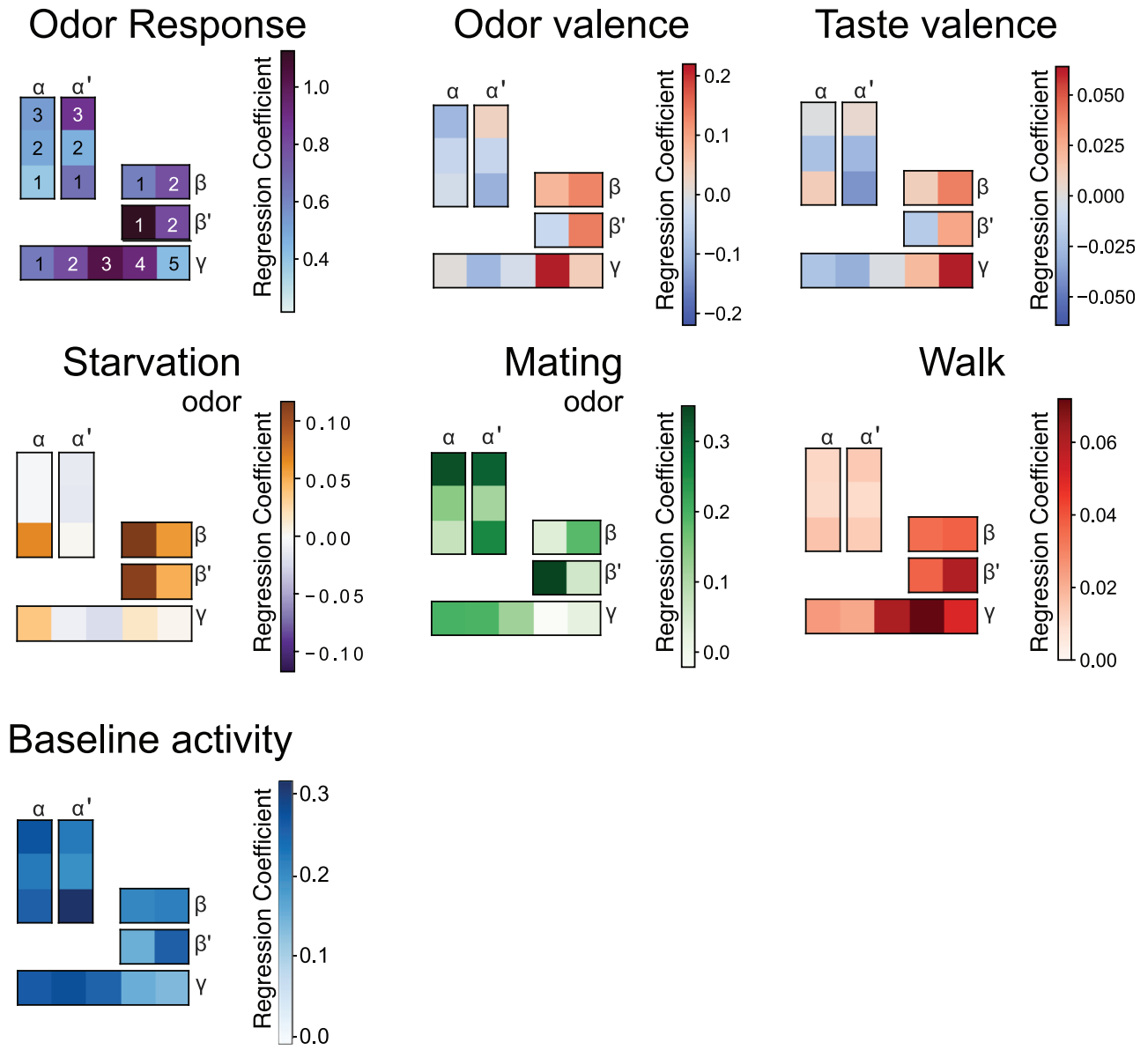

Figure 6. Summary Models of the Contribution of Different MB Compartments

Mushroom body compartments are color coded with the value of the regression coefficient. Different compartments could therefore contribute differentially to the perception of sensory valence and internal state. Note that panels "starvation" and "mating" display state-dependent modulation of odor responses. Differences in magnitude of regression coefficients stem from the use of slightly different genotypes (i.e., the graphics "taste valence" and "walk" represent data collected using flies with two copies of upstream activating sequence [UAS] and GAL4 transgenes, although data for all other graphics were collected with flies with one copy of each. This likely led to higher baseline fluorescence and thus a lower ΔF/F). See also Figure S6.

been observed in MBON responses by Hige et al. [39]. And similarly, manipulation of MBON or DAN output changes behavior in naive animals [13, 18, 47]. These innate biases in the MB network could in turn serve as a teaching signal for novel odors and change over an animal's lifetime or even over evolutionary times to thus contribute to species-specific behaviors.

In conclusion, we propose that DANs as a population govern innate perception and behavior by directly and differentially encoding the innate valence of a sensory cue and the animal's current physiological and behavioral state.

STAR★METHODS

Detailed methods are provided in the online version of this paper and include the following:

- KEY RESOURCES TABLE
- LEAD CONTACT AND MATERIALS AVAILABILITY
- EXPERIMENTAL MODEL AND SUBJECT DETAILS
  - Number of experiments
- METHOD DETAILS
  - Two-photon *in vivo* calcium imaging

- Odor stimulation
- Image analysis and 3D registration
- *In vivo* light field imaging experiments
- QUANTIFICATION AND STATISTICAL ANALYSIS
  - Statistics and other types of data analysis
  - Olfactory arena preference test
- DATA AND CODE AVAILABILITY

SUPPLEMENTAL INFORMATION

Supplemental Information can be found online at https://doi.org/10.1016/j.cub.2020.04.037.

ACKNOWLEDGMENTS

We would like to thank Sebastian Onasch and Ariane Böhm for their help with data analysis and modeling and Christian Schmid for writing the odor delivery script. We are grateful to Rüdiger Klein and the Max Planck Institute for Neurobiology for generously sharing their multiphoton microscope and to Robert Kasper for his technical help. This study was financed by the German Research Foundation (DFG) (SFB870 [A04] and FOR2705 [TP3]) and an ERC starting grant (FlyContext) to I.C.G.K. V.S. and R.P. were funded by the DFG under Germany's Excellence Strategy within the framework of the Munich Cluster for Systems Neurology (EXC 2145 SyNergy–ID 390857198). V.S., R.P., J.G., and I.C.G.K. received further funding from the Max-Planck-Society.

AUTHOR CONTRIBUTIONS

K.P.S. and I.C.G.K. conceived the study in collaboration with R.P. and V.S. K.P.S. carried out all *in vivo* two-photon imaging and all behavioral experiments. V.S. and R.P. designed the 3D image analysis method. K.P.S. and V.S. extracted the raw data from the two-photon experiments, and S.A., with the help of V.S., R.P., and J.G., analyzed the data and generated the models. S.A. carried out all light-field microscopy experiments and their analysis. I.C.G.K. wrote the manuscript with help and input from all authors.

DECLARATION OF INTERESTS

The authors declare no competing interests.

Received: October 15, 2019
Revised: March 13, 2020
Accepted: April 16, 2020
Published: May 7, 2020

REFERENCES

1. Sayin, S., Boehm, A.C., Kobler, J.M., De Backer, J.F., and Grunwald Kadow, I.C. (2018). Internal state dependent odor processing and perception-the role of neuromodulation in the fly olfactory system. Front. Cell. Neurosci. *12*, 11.
2. Lee, S.H., and Dan, Y. (2012). Neuromodulation of brain states. Neuron *76*, 209–222.
3. Bargmann, C.I., and Marder, E. (2013). From the connectome to brain function. Nat. Methods *10*, 483–490.
4. Volkow, N.D., Wise, R.A., and Baler, R. (2017). The dopamine motive system: implications for drug and food addiction. Nat. Rev. Neurosci. *18*, 741–752.
5. Schultz, W. (2015). Neuronal reward and decision signals: from theories to data. Physiol. Rev. *95*, 853–951.
6. Kaun, K.R., and Rothenfluh, A. (2017). Dopaminergic rules of engagement for memory in *Drosophila*. Curr. Opin. Neurobiol. *43*, 56–62.
7. Björklund, A., and Dunnett, S.B. (2007). Dopamine neuron systems in the brain: an update. Trends Neurosci. *30*, 194–202.
8. Mohebi, A., Pettibone, J.R., Hamid, A.A., Wong, J.T., Vinson, L.T., Patriarchi, T., Tian, L., Kennedy, R.T., and Berke, J.D. (2019). Dissociable dopamine dynamics for learning and motivation. Nature *570*, 65–70.
9. Van Swinderen, B., and Andretic, R. (2011). Dopamine in *Drosophila*: setting arousal thresholds in a miniature brain. Proc. Biol. Sci. *278*, 906–913.
10. Aso, Y., Sitaraman, D., Ichinose, T., Kaun, K.R., Vogt, K., Belliart-Guérin, G., Plaçais, P.Y., Robie, A.A., Yamagata, N., Schnaitmann, C., et al. (2014). Mushroom body output neurons encode valence and guide memory-based action selection in *Drosophila*. eLife *3*, e04580.
11. Aso, Y., Hattori, D., Yu, Y., Johnston, R.M., Iyer, N.A., Ngo, T.T., Dionne, H., Abbott, L.F., Axel, R., Tanimoto, H., and Rubin, G.M. (2014). The neuronal architecture of the mushroom body provides a logic for associative learning. eLife *3*, e04577.
12. Waddell, S. (2010). Dopamine reveals neural circuit mechanisms of fly memory. Trends Neurosci. *33*, 457–464.
13. Tsao, C.H., Chen, C.C., Lin, C.H., Yang, H.Y., and Lin, S. (2018). *Drosophila* mushroom bodies integrate hunger and satiety signals to control innate food-seeking behavior. eLife *7*, e35264.
14. Bouzaiane, E., Trannoy, S., Scheunemann, L., Plaçais, P.Y., and Preat, T. (2015). Two independent mushroom body output circuits retrieve the six discrete components of *Drosophila* aversive memory. Cell Rep. *11*, 1280–1292.
15. Sayin, S., De Backer, J.F., Siju, K.P., Wosniack, M.E., Lewis, L.P., Frisch, L.M., Gansen, B., Schlegel, P., Edmondson-Stait, A., Sharifi, N., et al. (2019). A neural circuit arbitrates between persistence and withdrawal in hungry *Drosophila*. Neuron *104*, 544–558.e6.
16. Mao, Z., and Davis, R.L. (2009). Eight different types of dopaminergic neurons innervate the *Drosophila* mushroom body neuropil: anatomical and physiological heterogeneity. Front. Neural Circuits *3*, 5.
17. Heisenberg, M. (2003). Mushroom body memoir: from maps to models. Nat. Rev. Neurosci. *4*, 266–275.
18. Lewis, L.P., Siju, K.P., Aso, Y., Friedrich, A.B., Bulteel, A.J., Rubin, G.M., and Grunwald Kadow, I.C. (2015). A higher brain circuit for immediate integration of conflicting sensory information in *Drosophila*. Curr. Biol. *25*, 2203–2214.
19. Azanchi, R., Kaun, K.R., and Heberlein, U. (2013). Competing dopamine neurons drive oviposition choice for ethanol in *Drosophila*. Proc. Natl. Acad. Sci. USA *110*, 21153–21158.
20. Burke, C.J., Huetteroth, W., Owald, D., Perisse, E., Krashes, M.J., Das, G., Gohl, D., Silies, M., Certel, S., and Waddell, S. (2012). Layered reward signalling through octopamine and dopamine in *Drosophila*. Nature *492*, 433–437.
21. Aso, Y., Herb, A., Ogueta, M., Siwanowicz, I., Templier, T., Friedrich, A.B., Ito, K., Scholz, H., and Tanimoto, H. (2012). Three dopamine pathways induce aversive odor memories with different stability. PLoS Genet. *8*, e1002768.
22. Berry, J.A., Cervantes-Sandoval, I., Nicholas, E.P., and Davis, R.L. (2012). Dopamine is required for learning and forgetting in *Drosophila*. Neuron *74*, 530–542.
23. Keleman, K., Vrontou, E., Krüttner, S., Yu, J.Y., Kurtovic-Kozaric, A., and Dickson, B.J. (2012). Dopamine neurons modulate pheromone responses in *Drosophila* courtship learning. Nature *489*, 145–149.
24. Trannoy, S., Redt-Clouet, C., Dura, J.M., and Preat, T. (2011). Parallel processing of appetitive short- and long-term memories in *Drosophila*. Curr. Biol. *21*, 1647–1653.
25. Bang, S., Hyun, S., Hong, S.T., Kang, J., Jeong, K., Park, J.J., Choe, J., and Chung, J. (2011). Dopamine signalling in mushroom bodies regulates temperature-preference behaviour in *Drosophila*. PLoS Genet. *7*, e1001346.
26. Aso, Y., Siwanowicz, I., Bräcker, L., Ito, K., Kitamoto, T., and Tanimoto, H. (2010). Specific dopaminergic neurons for the formation of labile aversive memory. Curr. Biol. *20*, 1445–1451.

27. Liu, C., Plaçais, P.Y., Yamagata, N., Pfeiffer, B.D., Aso, Y., Friedrich, A.B., Siwanowicz, I., Rubin, G.M., Preat, T., and Tanimoto, H. (2012). A subset of dopamine neurons signals reward for odour memory in *Drosophila*. Nature *488*, 512–516.

28. Cohn, R., Morantte, I., and Ruta, V. (2015). Coordinated and compartmentalized neuromodulation shapes sensory processing in *Drosophila*. Cell *163*, 1742–1755.

29. Riemensperger, T., Völler, T., Stock, P., Buchner, E., and Fiala, A. (2005). Punishment prediction by dopaminergic neurons in *Drosophila*. Curr. Biol. *15*, 1953–1960.

30. Boto, T., Stahl, A., Zhang, X., Louis, T., and Tomchik, S.M. (2019). Independent contributions of discrete dopaminergic circuits to cellular plasticity, memory strength, and valence in *Drosophila*. Cell Rep. *27*, 2014–2021.e2.

31. Tomchik, S.M. (2013). Dopaminergic neurons encode a distributed, asymmetric representation of temperature in *Drosophila*. J. Neurosci. *33*, 2166–76a.

32. Hong, S.T., Bang, S., Hyun, S., Kang, J., Jeong, K., Paik, D., Chung, J., and Kim, J. (2008). cAMP signalling in mushroom bodies modulates temperature preference behaviour in *Drosophila*. Nature *454*, 771–775.

33. Eichler, K., Li, F., Litwin-Kumar, A., Park, Y., Andrade, I., Schneider-Mizell, C.M., Saumweber, T., Huser, A., Eschbach, C., Gerber, B., et al. (2017). The complete connectome of a learning and memory centre in an insect brain. Nature *548*, 175–182.

34. Takemura, S.Y., Aso, Y., Hige, T., Wong, A., Lu, Z., Xu, C.S., Rivlin, P.K., Hess, H., Zhao, T., Parag, T., et al. (2017). A connectome of a learning and memory center in the adult *Drosophila* brain. eLife *6*, e26975.

35. Zheng, Z., Lauritzen, J.S., Perlman, E., Robinson, C.G., Nichols, M., Milkie, D., Torrens, O., Price, J., Fisher, C.B., Sharifi, N., et al. (2018). A complete electron microscopy volume of the brain of adult *Drosophila melanogaster*. Cell *174*, 730–743.E22.

36. Ichinose, T., Aso, Y., Yamagata, N., Abe, A., Rubin, G.M., and Tanimoto, H. (2015). Reward signal in a recurrent circuit drives appetitive long-term memory formation. eLife *4*, e10719.

37. Zhao, X., Lenek, D., Dag, U., Dickson, B.J., and Keleman, K. (2018). Persistent activity in a recurrent circuit underlies courtship memory in *Drosophila*. eLife *7*, e31425.

38. Dolan, M.J., Frechter, S., Bates, A.S., Dan, C., Huoviala, P., Roberts, R.J., Schlegel, P., Dhawan, S., Tabano, R., Dionne, H., et al. (2019). Neurogenetic dissection of the *Drosophila* lateral horn reveals major outputs, diverse behavioural functions, and interactions with the mushroom body. eLife *8*, e43079.

39. Hige, T., Aso, Y., Rubin, G.M., and Turner, G.C. (2015). Plasticity-driven individualization of olfactory coding in mushroom body output neurons. Nature *526*, 258–262.

40. Campbell, R.A., Honegger, K.S., Qin, H., Li, W., Demir, E., and Turner, G.C. (2013). Imaging a population code for odor identity in the *Drosophila* mushroom body. J. Neurosci. *33*, 10568–10581.

41. Gottfried, J.A. (2010). Central mechanisms of odour object perception. Nat. Rev. Neurosci. *11*, 628–641.

42. Landayan, D., Feldman, D.S., and Wolf, F.W. (2018). Satiation state-dependent dopaminergic control of foraging in *Drosophila*. Sci. Rep. *8*, 5777.

43. Stensmyr, M.C., Dweck, H.K., Farhan, A., Ibba, I., Strutz, A., Mukunda, L., Linz, J., Grabe, V., Steck, K., Lavista-Llanos, S., et al. (2012). A conserved dedicated olfactory circuit for detecting harmful microbes in *Drosophila*. Cell *151*, 1345–1357.

44. Knaden, M., Strutz, A., Ahsan, J., Sachse, S., and Hansson, B.S. (2012). Spatial representation of odorant valence in an insect brain. Cell Rep. *1*, 392–399.

45. Strutz, A., Soelter, J., Baschwitz, A., Farhan, A., Grabe, V., Rybak, J., Knaden, M., Schmuker, M., Hansson, B.S., and Sachse, S. (2014). Decoding odor quality and intensity in the *Drosophila* brain. eLife *3*, e04147.

46. Semmelhack, J.L., and Wang, J.W. (2009). Select *Drosophila* glomeruli mediate innate olfactory attraction and aversion. Nature *459*, 218–223.

47. Owald, D., Felsenberg, J., Talbot, C.B., Das, G., Perisse, E., Huetteroth, W., and Waddell, S. (2015). Activity of defined mushroom body output neurons underlies learned olfactory behavior in *Drosophila*. Neuron *86*, 417–427.

48. Wang, Y., Guo, H.F., Pologruto, T.A., Hannan, F., Hakker, I., Svoboda, K., and Zhong, Y. (2004). Stereotyped odor-evoked activity in the mushroom body of *Drosophila* revealed by green fluorescent protein-based Ca2+ imaging. J. Neurosci. *24*, 6507–6514.

49. Aimon, S., Katsuki, T., Jia, T., Grosenick, L., Broxton, M., Deisseroth, K., Sejnowski, T.J., and Greenspan, R.J. (2019). Fast near-whole-brain imaging in adult *Drosophila* during responses to stimuli and behavior. PLoS Biol. *17*, e2006732.

50. Huetteroth, W., Perisse, E., Lin, S., Klappenbach, M., Burke, C., and Waddell, S. (2015). Sweet taste and nutrient value subdivide rewarding dopaminergic neurons in *Drosophila*. Curr. Biol. *25*, 751–758.

51. Yamagata, N., Ichinose, T., Aso, Y., Plaçais, P.Y., Friedrich, A.B., Sima, R.J., Preat, T., Rubin, G.M., and Tanimoto, H. (2015). Distinct dopamine neurons mediate reward signals for short- and long-term memories. Proc. Natl. Acad. Sci. USA *112*, 578–583.

52. Rolls, E.T. (2007). Sensory processing in the brain related to the control of food intake. Proc. Nutr. Soc. *66*, 96–112.

53. Soria-Gómez, E., Bellocchio, L., Reguero, L., Lepousez, G., Martin, C., Bendahmane, M., Ruehle, S., Remmers, F., Desprez, T., Matias, I., et al. (2014). The endocannabinoid system controls food intake via olfactory processes. Nat. Neurosci. *17*, 407–415.

54. Grunwald Kadow, I.C. (2019). State-dependent plasticity of innate behavior in fruit flies. Curr. Opin. Neurobiol. *54*, 60–65.

55. Krashes, M.J., DasGupta, S., Vreede, A., White, B., Armstrong, J.D., and Waddell, S. (2009). A neural circuit mechanism integrating motivational state with memory expression in *Drosophila*. Cell *139*, 416–427.

56. Hussain, A., Üçpunar, H.K., Zhang, M., Loschek, L.F., and Grunwald Kadow, I.C. (2016). Neuropeptides modulate female chemosensory processing upon mating in *Drosophila*. PLoS Biol. *14*, e1002455.

57. Das, S., Trona, F., Khallaf, M.A., Schuh, E., Knaden, M., Hansson, B.S., and Sachse, S. (2017). Electrical synapses mediate synergism between pheromone and food odors in *Drosophila melanogaster*. Proc. Natl. Acad. Sci. USA *114*, E9962–E9971.

58. Joseph, R.M., Devineni, A.V., King, I.F., and Heberlein, U. (2009). Oviposition preference for and positional avoidance of acetic acid provide a model for competing behavioral drives in *Drosophila*. Proc. Natl. Acad. Sci. USA *106*, 11352–11357.

59. Berry, J.A., Cervantes-Sandoval, I., Chakraborty, M., and Davis, R.L. (2015). Sleep facilitates memory by blocking dopamine neuron-mediated forgetting. Cell *161*, 1656–1667.

60. Honegger, K., and de Bivort, B. (2018). Stochasticity, individuality and behavior. Curr. Biol. *28*, R8–R12.

61. Schindelin, J., Arganda-Carreras, I., Frise, E., Kaynig, V., Longair, M., Pietzsch, T., Preibisch, S., Rueden, C., Saalfeld, S., Schmid, B., et al. (2012). Fiji: an open-source platform for biological-image analysis. Nat. Methods *9*, 676–682.

62. van der Walt, S., Schönberger, J.L., Nunez-Iglesias, J., Boulogne, F., Warner, J.D., Yager, N., Gouillart, E., and Yu, T.; scikit-image contributors (2014). scikit-image: image processing in Python. PeerJ *2*, e453.

63. Broxton, M., Grosenick, L., Yang, S., Cohen, N., Andalman, A., Deisseroth, K., and Levoy, M. (2013). Wave optics theory and 3-D deconvolution for the light field microscope. Opt. Express *21*, 25418–25439.

64. Abraham, A., Pedregosa, F., Eickenberg, M., Gervais, P., Mueller, A., Kossaifi, J., Gramfort, A., Thirion, B., and Varoquaux, G. (2014). Machine learning for neuroimaging with scikit-learn. Front. Neuroinform. *8*, 14.

STAR★METHODS

KEY RESOURCES TABLE

REAGENT or RESOURCE	SOURCE	IDENTIFIER
Antibodies		
Anti-Rabbit Alexa 488	Molecular Probes	RRID: AB_2576217
Anti-Mouse Alexa 568	Molecular Probes	RRID: AB_141372
Mouse monoclonal anti-discs large	DSHB	RRID: AB_528203
Rabbit polyclonal anti-GFP	Clontech	RRID: AB_2336883
Data		
2-photon 3D data analysis tool	Github	https://github.com/portugueslab/lobe_alignment
Light field data and analysis	Github	https://github.com/sophie63/Siju2020
Light field imaging data (walking)	crcns.org	https://doi.org/10.6080/K01J97ZN
Light field data analysis protocol	Github	https://github.com/sophie63/FlyLFM
All remaining original data are available upon request.		
Experimental Models: Organisms/Strains		
D.mel/TH-Gal4	Bloomington DSC	FlyBase: FBst0008848
D.mel/GMR58E02-Gal4	Bloomington DSC	FlyBase: FBst0041347
D.mel/TH,58E02-Gal4	This paper	N/A
D.mel/UAS-GCaMP6f	Bloomington DSC	FlyBase: FBst0042747
Software and Algorithms		
FV10-ASW	Olympus	olympus-lifescience.com
MATLAB	MATLAB	mathworks.com
FIJI	[61]	https://fiji.sc/#
Python		For details see method description
GraphPad Prism 8	GraphPad	https://www.graphpad.com

LEAD CONTACT AND MATERIALS AVAILABILITY

Further information and requests for resources, code, and reagents should be directed to and will be fulfilled by the lead contact, Ilona C. Grunwald Kadow (ilona.grunwald@tum.de).

EXPERIMENTAL MODEL AND SUBJECT DETAILS

All experiments were carried out with laboratory-raised *Drosophila melanogaster*. In order to cover both PPL1 and PAM DANs for imaging, we recombined two transgenic driver lines, namely the TH-Gal4 (PPL) driver and the 58E02-Gal4 (PAM) driver, onto the third chromosome. The recombined line was crossed to the UAS-GCaMP6f reporter line for *in vivo* imaging. For experiments using light field imaging, the additional data to the dataset from [49] was obtained with flies where the same TH- and 58E02-Gal4 drivers or TH- and DDC-Gal4 drivers were combined with the UAS-GCaMP6F transgene to obtain a true breeding stock. All fly stocks and crosses were raised on a standard cornmeal medium and maintained at 25°C and 60% humidity in 12 h light and 12 dark cycle climate chambers.

Number of experiments

'N' indicates the number of flies, and 'n' signifies the number of experiments. For two-photon imaging experiments: A total of 391 *in vivo* experiments were analyzed from 201 adult female flies of different states stimulated with different odors. (1) Vinegar: fed: n = 10, N = 8; starved: n = 30, N = 23; (2) Yeast: fed: n = 14, N = 11; starved: n = 30, N = 22; (3) Isoamyl acetate: fed: n = 12, N = 8; starved: n = 13, N = 10; (4) 1-Hexanol: fed: n = 8, N = 4 ; starved: n = 12, N = 8; (5) 2-Heptanone: fed: n = 9, N = 5; starved: n = 12, N = 8; (6) Ethanol: fed: n = 6, N = 4; starved: n = 7, N = 5; (7) 3-Octanol: fed: n = 8, N = 6; starved: n = 9, N = 7; (8) 4-MCH: fed: n = 11, N = 5; starved: n = 11, N = 9; (9) Peppermint: fed: n = 12, N = 8; starved: n = 13, N = 7; (10) Citronella: fed: n = 11, N = 8; starved: n = 38, N = 30; (11) Geosmin: fed: n = 9, N = 5; starved:

n = 6, N = 4; (12) cVA: mated: n = 38, N = 14; Virgin: n = 30, N = 14; (13) high vinegar: fed: n = 16, N = 8; starved: n = 16, N = 8. Odor stimulation was semi-randomized for different experiments and animals such that in an initial set of experiments with citronella, yeast and vinegar only these odors were randomized. In the second set of experiments, these odors and all remaining odors were presented in a randomized order.

For light field imaging experiments: walking experiments, N = 7; taste experiments, sucrose N = 10, quinine N = 9.

METHOD DETAILS

Two-photon *in vivo* calcium imaging

4- to 8-day-old female flies were used for all experiments. For starvation experiments, flies of at least 4 days old were transferred to a starvation bottle with only a wet tissue paper in the bottom and a folded wet Whatman round filter paper as a wick hanging from the plug. Starvation was carried out for 24 h or 48 h for the experiments.

For *in vivo* imaging, a fly was restrained in a truncated pipette tip and only a part of the head with antenna and maxillary palp were protruding (see Figure 1A). Proboscis and legs were kept inside the pipette tip to restrain movement. Using fine forceps, cuticle on the dorsal head was removed and the brain was further exposed by removing fat bodies and trachea. The exposed brain was first washed with imaging saline, and then a drop of 1% low temperature melting agarose (NuSieveGTG, Lonza) diluted in imaging saline maintained at 37°C was added on top of the brain in order to minimize brain movement. Imaging saline was added on top once the agarose had hardened. Preparations were imaged with an Olympus 40x 0.8 NA water immersion objective on an Olympus FV1000 two-photon system with a BX61WI microscope. GCaMP6f fluorescence was excited at 910 nm by a mode-locked Ti:Sapphire Mai Tai DeepSee laser. Time series images were acquired at 210 × 210 pixel resolution with 3 frames per s speed using the Olympus FV10-ASW imaging software. For each specimen, first the dorsal and ventral ends of mushroom body DANs were marked in the software. The entire volume of the MB from dorsal to ventral was ~100 μm. Planes were spaced 1 or 2 μm apart in all experiments. Each plane was scanned in time series mode for 80 frames with a speed of 3 frames per second to obtain sufficient spatial resolution for pre-, post- and stimulus phase. On each plane, a 1 s odor pulse was delivered at the 30th time frame by triggering an automated odor delivery system. After scanning one plane, the focus was shifted to the next plane and the stimulation protocol was repeated for every plane. For each fly, the full volume of the MB was first scanned from dorsal to ventral and then from ventral to dorsal. The type and sequence of odors was randomized over experiments. For instance, in one set of experiments, two different odors were used for the opposite scanning directions, whereas in another set of experiments, the same odor was used for both scanning directions. In some cases, if the fly was still fit, a third or even fourth odor was recorded.

Odor stimulation

The following odorants were used in the study: vinegar (Balsamic vinegar, Alnatura, Germany), yeast (Fermipan, Italy; 1g/5ml water), citronella, peppermint (both from Aura Cacia, USA), 3-octanol, ethanol, 4-methylcyclohexanol (MCH), geosmin (0.01% in paraffin oil), isoamyl acetate, 1-Hexanol, 2-Heptanone (all from Sigma-Aldrich, Germany), 11-cis-Vaccenyl acetate (cVA) (Pherobanks, the Netherlands). Odors were diluted in water or paraffin oil to 1% with the exception of yeast and geosmin according to their solubility. For high vinegar stimulation vinegar was diluted to 80% in water to reach 32 ppm. A custom-made odor delivery system with mass flow controllers (Natec sensors, Garching) controlled by a MATLAB script were used for odor delivery. Throughout the experiments, a charcoal filtered continuous air stream of 1,000 mL/min was delivered through an 8 mm Teflon tube positioned 10 mm away from the fly antenna. Odor was delivered into the main air stream by redirecting 30% of main air flow for 1 s through a head-space glass vial containing 5 mL of diluted odorant. The odor delivery was automatically triggered by counting the time frame output from the scanning microscope by a custom written MATLAB script.

Image analysis and 3D registration

After acquisition, each imaging plane was first registered in time to correct for within-plane shifts. Then, all the planes were aligned with each other to maintain between-plane continuity. Both registration steps were performed with standard methods implemented in the scikit-image Python package (register_translation) [62].

Due to the variability in GCaMP expression between MB compartments and flies and lack of significant landmarks in the region imaged, automatic registration was not possible. Therefore, to assign activity to lobes, we used a semi manual-procedure. The binary masks for lobes published by Aso et al. [11] were then converted to meshes and simplified with the vtk toolkit. Next, the Aso et al. reference MB was registered manually to a high-resolution reference volume of the line TH-Gal4/58E02-Gal4;UAS-GCaMP6f used in this study (Figure S7, step 1).

Since the mushroom body is a L-shaped structure, determining the location of three points in three dimensions is enough to specify the location, rotation, and scale while also allowing for bending between the α, and β and γ lobes. Using a custom graphical user interface tool three points were determined: at the ends of the lobes, and the point where α and γ lobes come together. The exact location of the registration point is not important for the alignment quality, as long as they are located at the same cell, axon bundle or other landmark feature in both stacks.

Once this correspondence was established, the same procedure was repeated between each imaging experiment and the high-resolution TH/58E02 reference (Figure S7, step 2). Finally, for each transformed lobe or compartment, time traces of all voxels belonging to it (determined with a ray-intersection method from the trimesh library (developed by Dawson-Haggerty et al. version

3.2.0 at https://trimsh.org/) were extracted and saved per plane (each plane being a separate repetition, Figure S7, step 3). The analysis pipeline can be found at https://github.com/portugueslab/lobe_alignment.

The developed tool provides several advantages over the Longair and Jefferies ImageJ plugin (https://imagej.net/Name_Landmarks_and_Register): it shows an interactive preview of the segmentation, works with mesh-, instead of voxel-defined regions and is significantly faster to use. The ease of use was an important issue given the several hundreds of stacks acquired through the experiments.

For imaging experiments on the light field microscope, landmark registration was performed with FIJI's landmark_registration plugin (http://imagej.net/Name_Landmarks_and_Register) with the template of MB compartments.

In vivo light field imaging experiments

Flies with two copies of reporter and Gal4 drivers were used in all experiments. Note that this background is likely to increase the baseline fluorescence compared to the other experiments. If the signal is close to saturation, this could explain the decrease in ΔF/F. Light field imaging was carried out as previously described [49]. Briefly, the walking fly and taste response experiments were performed on a custom-built light-field microscope using a microlens array to separate rays coming from different angles [63]. The resulting light field images have information about fluorescence at different depths, and deconvolution allowed us to reconstruct the volume. This thus allowed us to record the whole volume without scanning.

Four of the datasets from walking flies were previously published in Aimon et al. [49] and source data (https://doi.org/10.6080/K01J97ZN), and the additional three datasets for walk, as well as all the datasets for taste were obtained specifically for this study (Video S1) (https://github.com/sophie63/Siju2020). Our light field microscope was constituted of a Thorlabs Cerna system with a Leica HC FLUOTAR L 25x/0.95 objective and an MLA-S125-f10 microlens array (RPC photonics) for one walk datasets and one taste dataset, and MLA-S125-f12 microlens array (RPC photonics) for two walk datasets and four taste datasets. The microlens array was placed on the image plane, while the camera imaged the microlens array through 50 mm f/1.4 NIKKOR-S Nikon relay lenses. The light field images were recorded at 25 and 50 Hz with a scientific CMOS camera (Hamamatsu ORCA-Flash 4.0). The volumes were reconstructed offline, using a python program developed by [63] and available on github: https://github.com/sophie63/FlyLFM. The movement artifacts were removed by 3D registration using the 3dvolreg routine from AFNI, and the voxel time series were transformed to ΔF/F by subtracting and normalizing by a moving average over 20 s. Functional regions were then extracted using principal component analysis and independent component analysis to highlight landmarks that were used to align both MB hemisphere to anatomical masks from Aso et al., 2014 [11]. The average of the whole MB volume was calculated for normalization of the taste response, but, in cases where some landmarks could not be clearly identified, neighboring compartments were discarded. Walking was scored by hand as a binary measure of walking on a ball versus non-walking movements or no movement at all.

For taste response experiments, a 24 h starved, one to two days old female was head-fixed (as described in [49]). The base of the proboscis, but not the legs, was fixed to reduce movement artifacts in this experiment, but it was kept accessible and clean. In some experiments we removed the front legs or painted the eyes to ensure the specificity of the response. Saturated solutions of sucrose or quinine were alternatively presented to the proboscis (as drops or using imbibed tissue), with individual stimulus presentation followed by water to rinse the proboscis before the next stimulus presentation. Approximately 30% of the datasets did not present any detectable activity and were therefore discarded.

QUANTIFICATION AND STATISTICAL ANALYSIS

Statistics and other types of data analysis

To reduce noise, we averaged responses during four time points after odor onset. Since for the majority of recorded flies, only two odors per fly were recorded or analyzed, we suspected strong multicollinearity in the data. Indeed, variance inflating factors were high and sometimes infinite. After removing the fly identity factor, variance inflating factors were three or less (without considering interactions), indicating low multicollinearity. We thus removed fly identity from the analysis (however as described below, we performed a mixed model to verify that fly identity did not strongly affect regression coefficients).

We next performed ANOVA, using a model considering all remaining factors (stimulus, position in odor sequence, imaging direction, starvation state), as well as compartment-specific effects (Table 1). As variance explained by position in odor sequence (i.e., whether odor was applied first or second in the sequence) was small and non-significant, we removed this factor for further analysis. We used this model for estimating regression coefficients. Note that we used a strict confidence interval of 98%, to decrease false positives in comparison of regression coefficients to zero .:

"df_f ~ lobe*(stimulus+order_presented+dorsal_to_ventral_val)+starved:lobe-1".

As cross-validation indicated some overfitting (24% instead of 37% of variance explained out of sample data), we also performed an elastic net regularization. We also used a mixed model with fly identity as group, to account for any fly specific effects. For coefficients related to valence, the same models were used but replacing stimulus with valence and restricting the data to odors with innate valence (vinegar, yeast, citronella, geosmin, and peppermint or vinegar, yeast, citronella, geosmin, peppermint, 3-octanol and 4-methylcyclohexanol). Finally, we estimated coefficients using minimal models for lobe ("df_f ~ lobe-1"), starvation ("df_f ~ lobe+lobe:starved-1"), and valence ("df_f ~ lobe+lobe:valence-1"). The coefficients for all the models are in good agreement

(Figures S1, S3, and S4). As cVA was the only odor recorded in the presence of different mating states, we used a simple model ("df_f ~ lobe+lobe:virgin_val-1") on this data subset to evaluate coefficients related to mating. For baseline analysis (pre-stimulus phase), we used the average of the deviation from zero. We also performed post hoc pairwise t tests for lobe specific effects of starvation, starvation baseline, odor valence, high and low vinegar, and mating. No pairwise comparison was carried out on the pre-stimulus of the mated versus virgins experiments, because the ANOVA, in contrast to the odor response for mating effect, showed no significant compartment-specific effects. All p values were pooled and corrected for multiple comparison using a Simes-Hochberg procedure. Regression coefficients for taste valence were also obtained using a simple model similar to the model used for odor valence. As the overall response was very variable (possibly due to fly identity or slight differences in the manual stimulus presentation), we also added the overall averaged activity into the model ("df_f~Mean+lobe+lobe:taste-1"). For walking experiments, we obtained behavior time series by binary scoring of walking on the ball. Those time series were convolved with a GCaMP6f kernel and the moving average was subtracted to match the ΔF/F of the fluorescence time series. Finally, it was normalized to have an average value of one during walk (to be able to compare regression coefficients with other factors with 0 or 1 values). We then performed regression of compartment averaged time series with these behavior time series to obtain regression coefficients. The ANOVA and regression analysis were performed using statsmodels (http://statsmodels.sourceforge.net/).

To see whether the fly can theoretically decode compartment activity to get information about stimulus, valence or starvation state, we trained logistic regression classifiers (lbfgs solvers for all, and balance class weight and multinomial logistic model for stimulus decoding). We also projected the data to obtain one to three dimensions using linear discriminant analysis. For valence or starvation, we evaluated separability using the d', and determined their p values using the distribution obtained by running LDA one thousand times on data with randomized valence or starvation state. For stimuli identity, we used the three first loadings to construct the odor space in Figure 2. The LDA and classification were performed using scikit-learn [64].

Olfactory arena preference test

Behavioral experiments with vinegar were conducted using a custom-built 4-arm olfactory choice arena described in Sayin et al. [15]. We used 4-8 days old *TH-Gal4,58E02-Gal4;UAS-GCaMP6f* flies for all behavioral experiments to match the genetic background of the flies used for imaging. All flies were starved for 24 h prior to the experiments. In each experiment, 20 to 30 flies of both sexes were used. We used a protocol consisting of 60 s pre-stimulus period, 90 s stimulus period, 210 s inter-stimulus period followed by another 90 s stimulus period. In one set of experiments, the odor headspace from either a 1% or an 80% vinegar solution was used to fill two opposite quadrants, and simultaneously the remaining two quadrants were filled with the odor of the solvent water (0% vinegar). In another set of experiments, two opposite quadrants were filled with 1% vinegar odor and simultaneously the remaining two quadrants were filled with 80% vinegar odor. In all the experiments, during the second stimulus phase of the protocol, stimuli were reversed with respect to the quadrants (see Figure 3E). The preference index was calculated as ((number of flies in Q1+Q3) (number of flies in Q2+Q4)/ total number of flies). Data were plotted in GraphPad Prism 8.

DATA AND CODE AVAILABILITY

The datasets and codes generated for the current study are either deposited in a public repository or are available directly from the lead contact on request, Ilona C. Grunwald Kadow (ilona.grunwald@tum.de).